CONF-9507182--

FUSION RESEARCH CENTER

DOE/ER/54241-154 FRCR #474

PAPERS PRESENTED AT THE 22ND EUROPEAN PHYSICAL SOCIETY CONFERENCE ON CONTROLLED FUSION AND PLASMA PHYSICS

Roger D. Bengtson, D. L. Brower, K. W. Gentle,
Yuri Y. Karzhavin, W. L. Rowan, and A. J. Wootton

Bournemouth, United Kingdom
July 3-7, 1995

THE UNIVERSITY OF TEXAS

Austin, Texas

Study of plasma edge turbulence via conditional probability density functions

Roger D. Bengtson, A. V. Filippas, and E. J. Powers
The University of Texas at Austin, Austin, Texas 78712 USA

1. Introduction

In experimental studies of plasma turbulence, knowledge of the probability density function (PDF) and the associated moments such as skewness and kurtosis can provide insight into the Gaussianity, or departure from Gaussianity of the plasma fluctuations. Gaussianity provides, via the central limit theorem, an estimate of the extent to which the commonly invoked random phase approximation is valid. Departures from a Gaussian PDF could be associated with nonlinear wave or mode coupling, or possibly the presence of coherent structures. Further insights of Gaussian statistics can be obtained from the joint PDF which describes the joint statistics at two points in space. Experimental joint PDF's using histogram-based techniques require a large amount of experimental data. For this reason, we have chosen, as an initial step in quantifying the joint statistics of edge turbulence, to estimate conditional PDF's. We compare the experimentally generated conditional PDF's with the theoretical conditional PDF for joint Gaussian statistics.

2. Statistical analysis

For a Gaussian random variable, the PDF is given by [1]

$$p(x) = \frac{e^{-(x-\eta)^2/2\sigma_x^2}}{\sqrt{2\pi}\sigma_x}, \qquad (1)$$

where x is the random variable, η is its mean, and σ_x^2 is its variance. For two Gaussian random variables, x and y, the joint probability density function is

$$p(x,y) = \frac{1}{2\pi\sigma^2\sqrt{1-\rho^2}} e^{\frac{-(x^2-2\rho xy+y^2)}{2\sigma^2(1-\rho^2)}} \qquad (2)$$

where $\sigma_x=\sigma_y=\sigma$, ρ is the correlation coefficient between x and y, and $\eta_x=\eta_y=0$. The conditional probability density function (CPDF) is the probability density function for a random variable x, when a condition is specified for the variable y and is given by . $p(x|y) = \frac{p(x,y)}{p(y)}$. For two zero mean Gaussian signals, the CPDF is given by

$$p(x|y) = \frac{1}{\sigma\sqrt{2\pi(1-\rho^2)}} e^{\frac{-(x-\rho y)^2}{2\sigma^2(1-\rho^2)}} \quad . \qquad (3)$$

Note that this corresponds to a Gaussian distribution with a mean $\eta_C = \rho y$ and variance $\sigma_c^2 = \sigma^2\left(1-\rho^2\right)$.

3. Experiment

The experiments [2] were conducted on the TEXT-U tokamak with plasma conditions $B_T = 2$ T, $I_p = 200$ kA, and a chord averaged density $n_e = 2.5 \times 10^{19} m^{-3}$ with hydrogen as a working gas. Two Langmuir probes, a stationary reference probe, and a moveable probe, with a separation in the poloidal direction were used in the scrape off layer and edge plasma of TEXT-U to measure the floating potential during the flat top region of the tokamak discharge. The probes were mounted on the top of the tokamak, displaced toroidally from the limiters (r=0.27 m) in the plasma current direction, and were moved in the radial direction between shots. The analysis assumes that statistically the shots are reproducible, and that the relevant statistical parameters do not change during a shot nor do they change from shot to shot. There are uncertainties in relating plasma potential fluctuations, ϕ_p, to the floating potential measurements since $\phi_p = \phi_f + \alpha T$, where α is a factor of order 2-3 and T is the plasma temperature. Earlier experiments have shown that under the conditions of this experiment, the amplitude of the temperature fluctuations [3] are typically half that of the density fluctuations and potential fluctuations. However, the statistics of the density, plasma potential, floating potential, and temperature fluctuations were similar [4] with nearly Gaussian PDF's, skewness approximately zero, and a kurtosis near 3. It is not clear how the present analysis is affected by ignoring temperature fluctuations. The floating potential signal was digitized at 2 MHz with a 12 bit digitizer with more than 250000 points per probe record.

4. Results

Figure 1 shows a characteristic PDF of the floating potential at the radial position r=0.27 m, near the shear layer[5], with a skewness S = -0.3 and kurtosis K = 3.2. Note that the largest deviations from a Gaussian PDF are for large amplitude fluctuations. In Figure 2 we show the experimental conditional probability density functions for the condition $\phi_C = -2.0\sigma$ on the reference probe at the same radial position, r=0.27 m used in figure 1 along with the functions as calculated using (3), where both the experimental CPDFs and the Gaussian CPDF were calculated for a time shift, τ, corresponding to the shift of the peak of the correlation coefficient function ρ. Moving along the peak of the correlation coefficient removes the E_rxB bulk rotation associated with the radial electric field. Poloidal separations of the moveable probe out to 59 mm are presented, while the poloidal correlation length for this data was 20 mm and a lifetime of 12×10^{-6}sec. Note that at this large condition, $\phi_C = -2.0\sigma$, the data set is small [9000 points] and the CPDF is noisier than the PDF in figure 1. Even at these extreme conditions, there is excellent agreement between the experimental CDPF and the CDPF calculated with Gaussian statistics. The CPDF relaxes back to the Gaussian distribution for a

single variable at a poloidal separation approximately twice the poloidal correlation length. The data presented here are representative of the data at all radial positions [2].

It has been pointed out that stronger deviations [6] from a Gaussian PDF will be observed for the vorticity variable than for the potential. Unfortunately we are not able to measure the vorticity.

We have demonstrated that the floating potential fluctuation statistics in the scrape off layer and edge plasma are nearly Gaussian. In addition, for two floating potential signals, the statistics can be described by a joint Gaussian distribution as is demonstrated by the conditional probability density function. This means that all of the fluctuating properties can be determined from the mean, standard deviation, and correlation ρ, and, given a condition on one probe, the PDF for a second probe can be described by a conditional Gaussian PDF.

Research supported in part by Department of Energy grant No. DE-FG05-88ER-53267.

References

[1] J. S. Bendat and A. G. Piersol, *Random Data: Analysis and Measurement Procedures*, 2nd ed. (Wiley, New York, (1986)

[2] Filippas, A. V., Bengtson, R. D, *et al*, Phys. Plasmas **2**, 839 (1995)

[3] H. Lin, R. D. Bengtson, and Ch. P. Ritz, Phys. Fluids B **1** 2027 (1989); H. Lin, G.-X. Li, R. D. Bengtson, Ch. P. Ritz, and H. Y. W. Tsui, Rev. Sci. Instrum. **63**, 4611 (1992)

[4] B. Metcalf, Undergraduate Thesis, Physics Department, University of Texas at Austin. (1994)

[5] Ch. P. Ritz, R. D. Bengtson, S. J. Levinson, and E. J. Powers, Phys. Fluids **27**, 2956 (1984)

[6] A. E. Koniges, J. A. Crotinger, and P. H. Diamond, Phys. Fluids B **4**, 2785 (1992), J. A. Crotinger, and T. H. Dupree, Phys. Fluids B **4**, 2854 (1992), and A. Das and P. Kaw, Phys. Plasmas **2**, 1497 (1995)

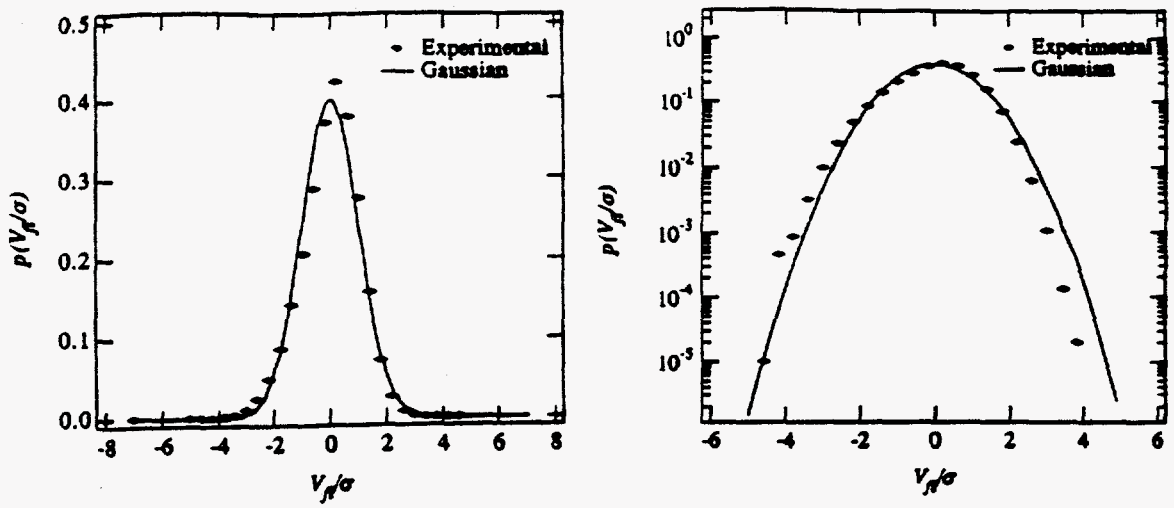

Figure 1. Probability density function at the radial position r = 0.27 m plotted on a linear and log scale. A Gaussian (solid line) is plotted for reference. S = -0.3, K = 3.2.

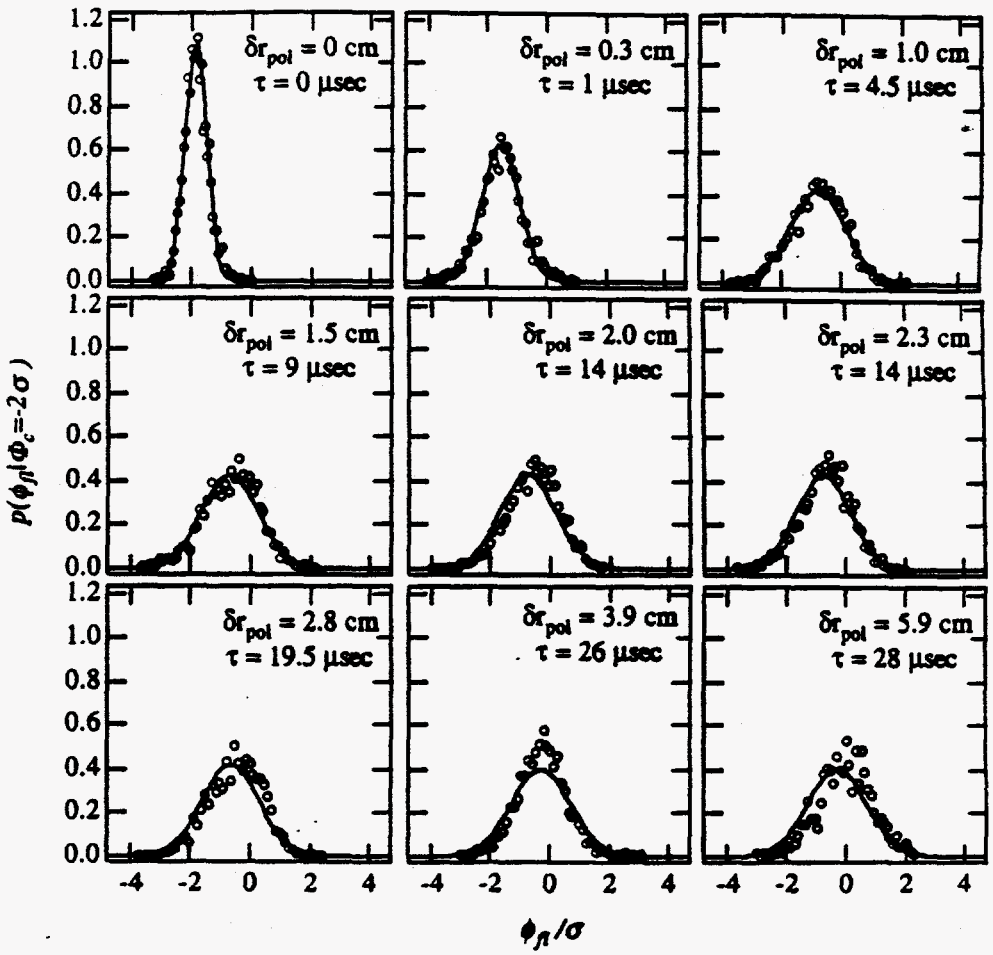

Figure 2 **Conditional probability density functions at radial position r = 0.27m for the movable probe at poloidal separations δr = 0,0.3,1,1.5,2,2.3,2.8,3.9,5.9 cm, for the condition ϕ_c= -2.0σ on the reference probe. The experimental data is plotted as points while the Gaussian estimate of the CPDF is shown as a solid line.**

CURRENT DENSITY PROFILE MEASUREMENT AND CURRENT DIFFUSION EXPERIMENTS ON TEXT-UPGRADE

D.L. Brower, Y. Jiang, L. Zeng, G. Cima[1], H. Gasquet[1], J. Lierzer[2], P.E. Phillips[1], B.W. Rice[3], D.R. Roberts[1], D.C. Sing[1], R. Steimle[1], A.J. Wootton[1]

Electrical Engineering Department, and Institute of Plasma and Fusion Research, University of California, Los Angeles, California 90095-1594, USA

[1] Fusion Research Center, The University of Texas, Austin, Texas, USA
[2] Nuclear Engineering Department, MIT, Cambridge, Massachusetts, USA
[3] Lawrence Livermore National Laboratory, Livermore, California, USA

Introduction: The UCLA far-infrared vertical-view multichannel heterodyne interferometer[1] on TEXT-Upgrade has recently been modified to include a polarimetry capability for measurement of the plasma current density profile. The interferometer/polarimeter consists of 15 chords with 3 cm spacing betweeen channels. The poloidal field is determined by measuring the Faraday rotation of the FIR laser beam through the plasma according to the technique of Rice[2]. The polarimeter has a 3 mrad rms noise level and 1 msec temporal resolution. The entire array can be translated across the plasma on a shot-to-shot basis allowing an increase in the number of chords for inversion. Equilibrium profiles have been measured for plasma discharges with varying edge q_a. Measured current density profiles are consistent with expectations from classical Spitzer conductivity. It is observed that $q_o < 1$ for sawtoothing discharges. In addition, evolution of the current density profile during electron cyclotron resonance heating and fast current ramps is explored. Profile modification due to large-amplitude tearing modes and locked modes are also addressed.

Equilibrium Profiles: Typical single-shot 15 channel polarimeter/interferometer data are shown in Fig. 1 for a TEXT-Upgrade limiter plasma with $B_T = 2.23\ T$, $I_p = 240\ kA$ and central density $n_{e0} = 3.8 \times 10^{19}\ m^{-3}$. Figures 1 (a) and (e) show the actual line-integrated polarimeter and interferometer profiles for a given point in time during the discharge. The maximum Faraday rotation angle measured here is about 6^o. To obtain the poloidal field as shown in Fig. 1(b), the line-integrated density and Faraday rotation profiles are inverted in a manner consistent with the Grad-Shafranov equilibrium to first order in the inverse aspect-ratio expansion. The current density profile, computed from Ampere's Law $J = \nabla \times B/\mu_o$, and safety factor are plotted in Figs. 1 (c) and (d), respectively. In general, good agreement is found between the measured current profile and that predicted from classical Spitzer conductivity. For this sawtoothing discharge the central safety factor $q_o = 0.85 \pm 0.10$. In general, for sawtoothing ohmic plasmas on TEXT-Upgrade, $0.80 \leq q_o \leq 1.0$. The sawtooth inversion radius, as determined from a soft x-ray array, corresponds to the point just inside $q = 1$ in Fig. 1(d). No modulation corresponding to the sawtooth cycle is observable on the time traces. In addition, ECE measurements of electron temperature fluctuations associated with small-amplitude m=2 tearing modes are in agreement with the location of the $q = 2$ surface from Fig. 1(d). For a given discharge, q_o falls below one at the onset of sawtoothing activity as shown in Fig. 2. Here sawteeth appear at approximately 80 msec which corresponds to $q_o \leq 1$ within the error bars of ± 0.10. Nonsawtoothing discharges occur at large q_a and are observed to have $q_o > 1$.

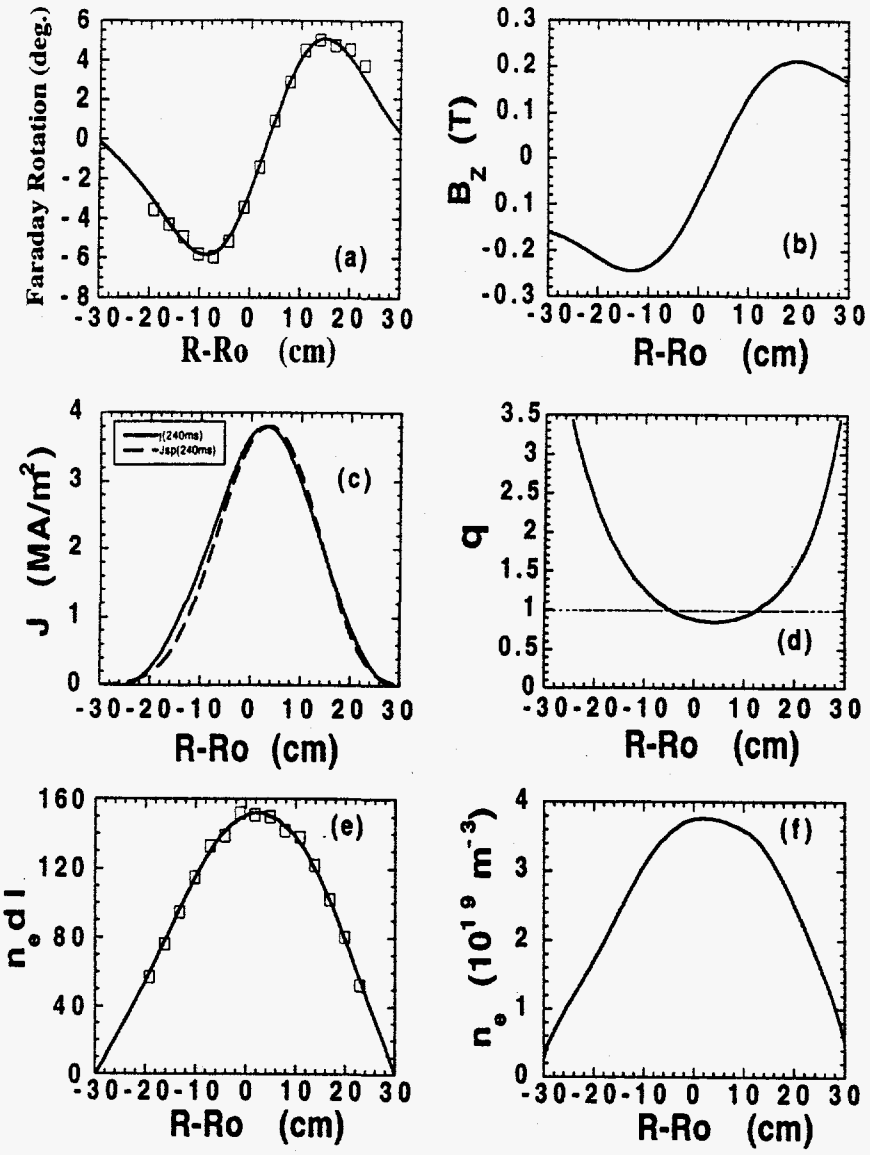

Figure 1. Single-shot 15 channel polarimeter/interferometer data showing (a) the Faraday rotation profile, (b) vertical component of the poloidal magnetic field, (c) current density profile which corresponds to the solid line in (a) [The dashed line represents the current density profile consistent with Spitzer conductivity], (d) tokamak safety factor, (e) chord-averaged electron density profile, and (f) inverted density profile. $R - R_o$ corresponds to the vacuum vessel center.

ECRH Modification of Current Density Profile: Electron Cyclotron Resonance Heating [ECRH] is employed on TEXT-Upgrade to heat the plasma electrons. Typically, large changes to the central electron temperature and sawtooth perturbation are observed during ECRH. In Fig. 3, an ohmic nonsawtoothing discharge with $B_T = 2.1\ T$ and $I_p = 150\ kA$ is heated on axis with ECRH. During the ECRH, at approximately 275 msec, sawteeth are observed and from the polarimeter data it is seen that this corresponds to q_o dropping below 1. Modification to the plasma current density profile during ECRH is also shown in Fig. 3. As the current density profile peaks, the central q value drops. These data are for high q_a plasmas where the heating region is comparable to the inversion radius. For low q_a discharges, where the sawtooth inversion radius is much larger than the ECR heating region, observed changes to the current density profiles are smaller.

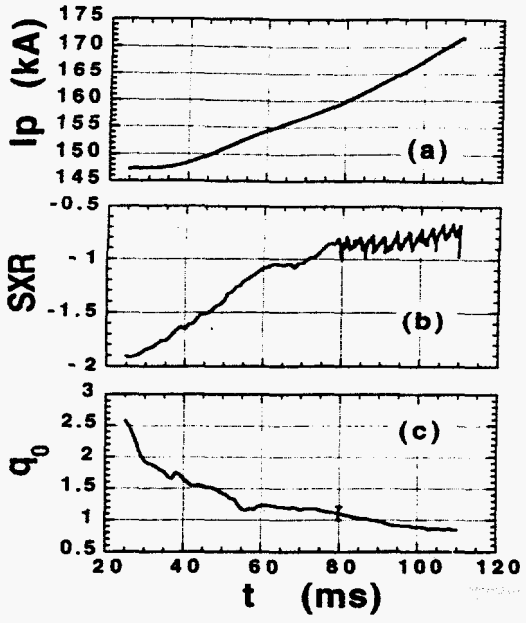

Figure 2. Response of (b) q_o and (c) soft x-ray [SXR] detectors to (a) current ramp during discharge start-up.

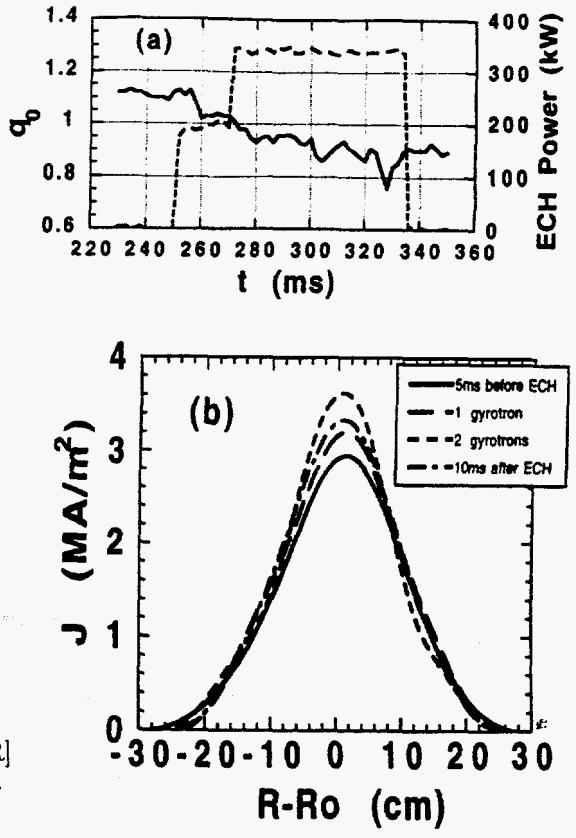

Figure 3. (a) Change in q_o [solid line] during ECRH [dashed line]. (b) Evolution of the current density profile during ECRH.

Fast Current Ramps and Current Diffusion: Fast plasma current ramps [5-8 MA-s^{-1}] are induced on TEXT-Upgrade in order to investigate current diffusion. In the example provided, the plasma current is ramped from 150 to 240 kA on a time-scale (16 msec) much faster than the classical skin time (100 msec). Preliminary data showing the evolution of the current density profile during this pertubation are provided in Fig. 4. A clear shoulder is observed on the current density profile during the current ramp phase from 200 to 220 msec. Using the measured $J(r,t)$ and $B_\theta(r,t)$, we can solve Ohm's law $\eta(r,t) = E(r,t)/J(r,t)$ directly for η where $E_T(r,t)$ is determined from Faraday's law. Using Spitzer resistivity, $\eta \propto A_z(r,t)T_e^{-3/2}ln\Lambda$ and the measured T_e profile, we can solve for A_z which is a function containing $Z_{eff}N(Z_{eff})$ plus any neoclassical or anomalous resistivity effects. For equilibrium plasmas, A_z is an indication of the plasma Z_{eff}. Evolution of the parameters $E_T(r,t)$ and $A_z(r,t)$ are shown in Figs. 4 (b) and (c), respectively. During the current ramp, a large change in A_z is indicated suggesting anomalous effects. Future work will include solving the current diffusion equation for these data.

One goal of these experiments is to increase the current ramp such that a hollow current density profile is achieved. In addition, ECRH heating will be employed to modify the internal inductance profile during these fast current ramps in order to sustain the perturbed profile. Plasma stability and confinement will then be examined under these different operating scenarios. The evolution of the current density profile during the plasma discharge turnon or breakdown phase will also be examined.

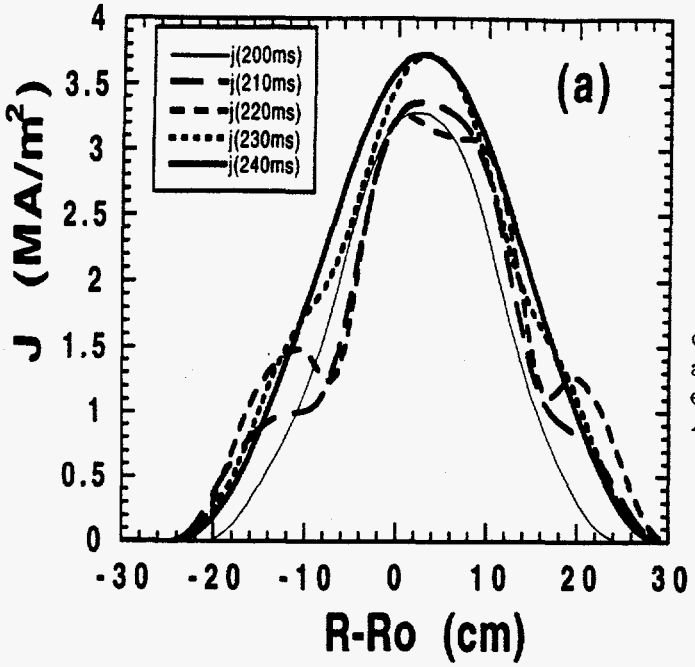

Figure 4. (a) Evolution of the current density profile during a fast I_p ramp. (b) and (c) Corresponding changes to toroidal electric field E_T and impurity parameter A_z, respectively.

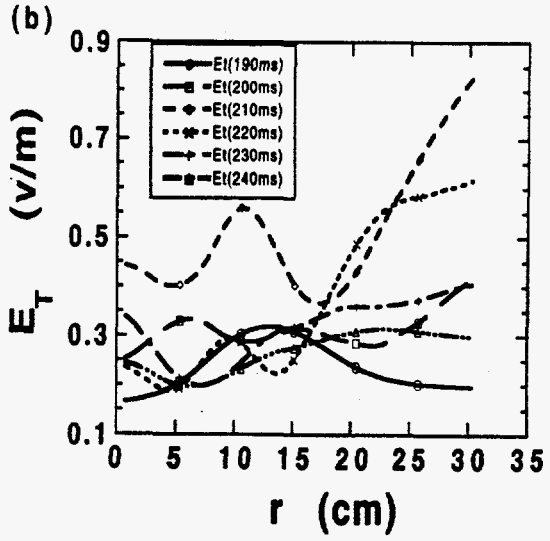

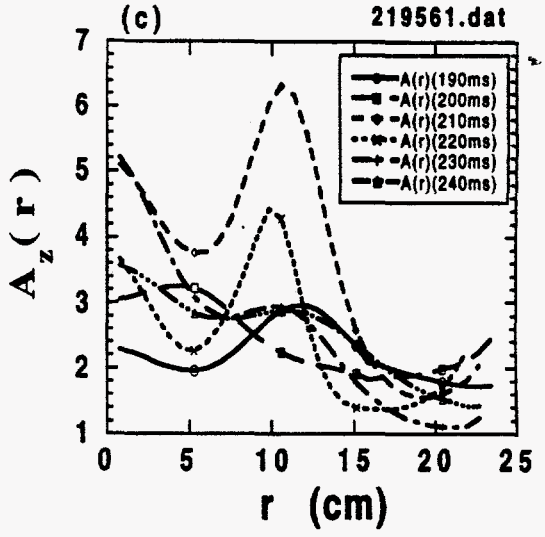

Tearing Modes, Locked Modes and Disruptions: Modification to the current density profile is observed during periods of large tearing mode activity and MARFEs. In both cases, fluctuations are clearly observed on the polarimeter signals and not on the interferometer, thereby indicating the origins are magnetic. Changes in the current density profile during these phenomena plus locked modes and disruptions will be the focus of future investigations.

Acknowledgements: This research is supported by U.S. Department of Energy under grants No. DE-FG03-86ER-53225, Task III and No. DE-AC05-78ET-53043.

[1] D.L. Brower, Y. Jiang, W.A. Peebles, S. Burns, N.C. Luhmann, Jr., Rev. Sci. Instrum. **63**,4990(1992).

[2] B.W. Rice, Rev. Sci. Instrum. **63**,5002(1992) and B.W. Rice, E.B. Hooper, Nucl. Fusion **34**,1(1994).

Nonlocal Transport Effects in Tokamak Electron Temperature Responses

K.W. Gentle, G. Cima, P.E. Phillips, W.L. Rowan, C. Watts, and A.J. Wootton
Fusion Research Center, University of Texas at Austin, Austin, Texas 78712

Although the presumption of local transport has proven most useful for many years, recent analysis of transients is suggesting limits to its validity. The electron temperature response of a tokamak discharge to a sharp increase in edge radiation has been found to differ significantly in TEXT from that expected from typical local transport models [1,2]. The response is best described by a nonlocal change in transport coefficients, as is necessary to explain the L-H transition in JET [3]. The nonlocal feature in TEXT is quite distinctive -- strong edge cooling is associated with a prompt rise in core temperatures. Quantitative analysis requires an increase in transport in the outer regions as well as a decrease in the core. This requires some kind of nonlocal coupling in transport mechanisms, and it also suggests some sort of global constraint or conservation principle to link increases in one location with decreases elsewhere. One candidate with a long tradition in tokamaks is the current or current profile.

To explore this possibility, an inverse experiment was undertaken: The response of the electron temperature to strong edge heating was examined. As in the earlier experiments, electron temperature was measured with a 16-channel heterodyne ECE system that covers the full profile. The edge heating was ohmic, produced by applying a voltage pulse to the ohmic windings and raising the plasma current. The initial discharge had high q, thus minimizing sawteeth and also providing a useful confirmation of current penetration time, judged by the appearance of strong sawteeth.

A typical voltage pulse is shown in Fig.1. An increase of 20 V in the loop voltage raised the current from 120 kA to 180 kA in ~ 10 msec. The density (central chord) increases slightly on a slow time scale from an initial line averaged value of 1.6×10^{19} m^{-3}. The plasma position is carefully controlled to within a few millimeters. Most remarkable, the central temperature initially drops by almost 20% within 5 msec before recovering. The core heating is delayed approximately 30 msec from the start of the voltage pulse, and regular sawteeth require 40 msec for initiation. The time histories of temperatures over the whole

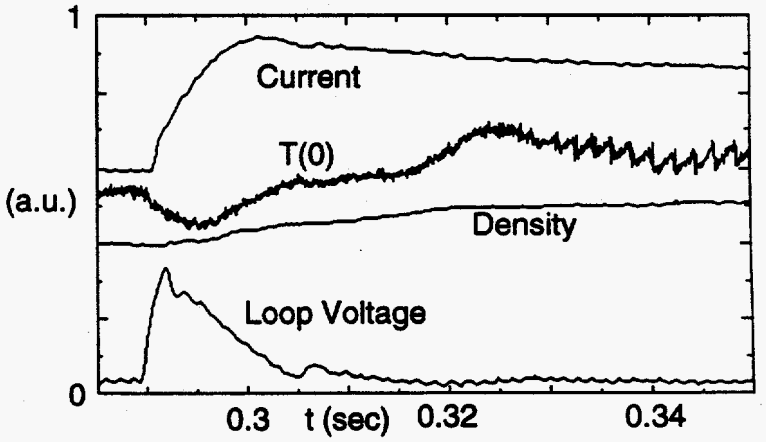

Fig. 1 A fast current increase in TEXT

profile in this case are shown in Fig. 2. The ECE channels at various $\rho = r/a$ for this circular, limited plasma with a = 0.27 m are shown. The channels at larger ρ than plotted show a fast response to the voltage pulse, but lack of opacity in the initial cold state prevents their interpretation as temperature. (However, there is no overshoot in those signals as could occur if the transient high E produced superthermals.) The experimental data are shown in heavy (noisy) lines in Fig. 2; the results of a heuristic model (discussed below) are shown as light (smooth) curves.

As the first step in the analysis of the experiment, the magnetic diffusion equation was solved using the measured current for the boundary condition, the measured temperature profiles to give the resistivity profiles, and a constant Z_{eff} to match the initial loop voltage. (The required surface voltage was less than that shown in Fig. 1 because the measuring loops are at r ~ 0.34 m.) The results are consistent with the qualitative features of Fig. 1 in requiring ~ 25 msec before significant changes occur in the core and ~ 50 msec to reach a new equilibrium. Although the current density rises rapidly at the edge, the drive is not sufficient to produce an inverted profile -- $j(\rho)$ remains monotonically decreasing throughout. The calculation provides the ohmic power $P(\rho,t)$ dissipated as needed for transport calculations.

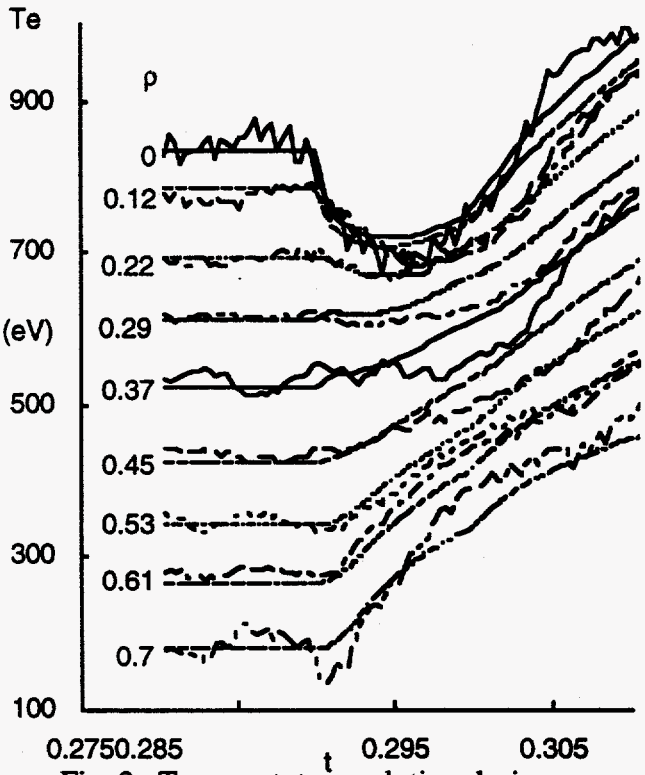

Fig. 2. Temperatutre evolution during a fast current ramp

The transport analysis for electrons includes ohmic input, radiative losses, and a $\chi_e(\rho)$ chosen to match the initial temperature profile. For these low densities, the energy transfer to ions is ignored as a small effective correction to radiation losses. The analysis is one-dimensional in the cylindrical coordinate ρ. The time-dependent case is modeled with the inferred ohmic $P(\rho,t)$ and various simple parameterizations for $\chi_e(\rho,t)$. The parameters are then adjusted for a reasonable semi-quantitative fit to the experimental $T_e(\rho,t)$. The prompt initial temperature drop in the core can only be produced by an increase in χ_e there in these circumstances. (In fact, the modeling is fairly subtle. If χ_e is merely increased in the core, the

temperature just outside would transiently rise as the energy is moved out of the core. In general, the whole $\chi_e(\rho)$ must be treated.) The temporary increase of χ_e in the core lasts only ~ 10 msec. Another remarkable feature, revealed only by quantitative analysis, is a reduction in χ_e the region of increased j. The temperature increases in this region are significantly greater than would be produced only by the increase in $P(\rho)$. The results of a model that reproduces the principal features of $T_e(\rho,t)$ in Fig. 2 is shown there with light smooth lines. The $\chi_e(\rho,t)$ of that model is shown in Fig. 3, which includes both the transient increase in core χ_e as well as the decrease in edge χ_e. (The true $\chi_e(\rho)$ increases faster toward the edge by the factor $n(0)/n(\rho)$, which is suppressed for clarity.)

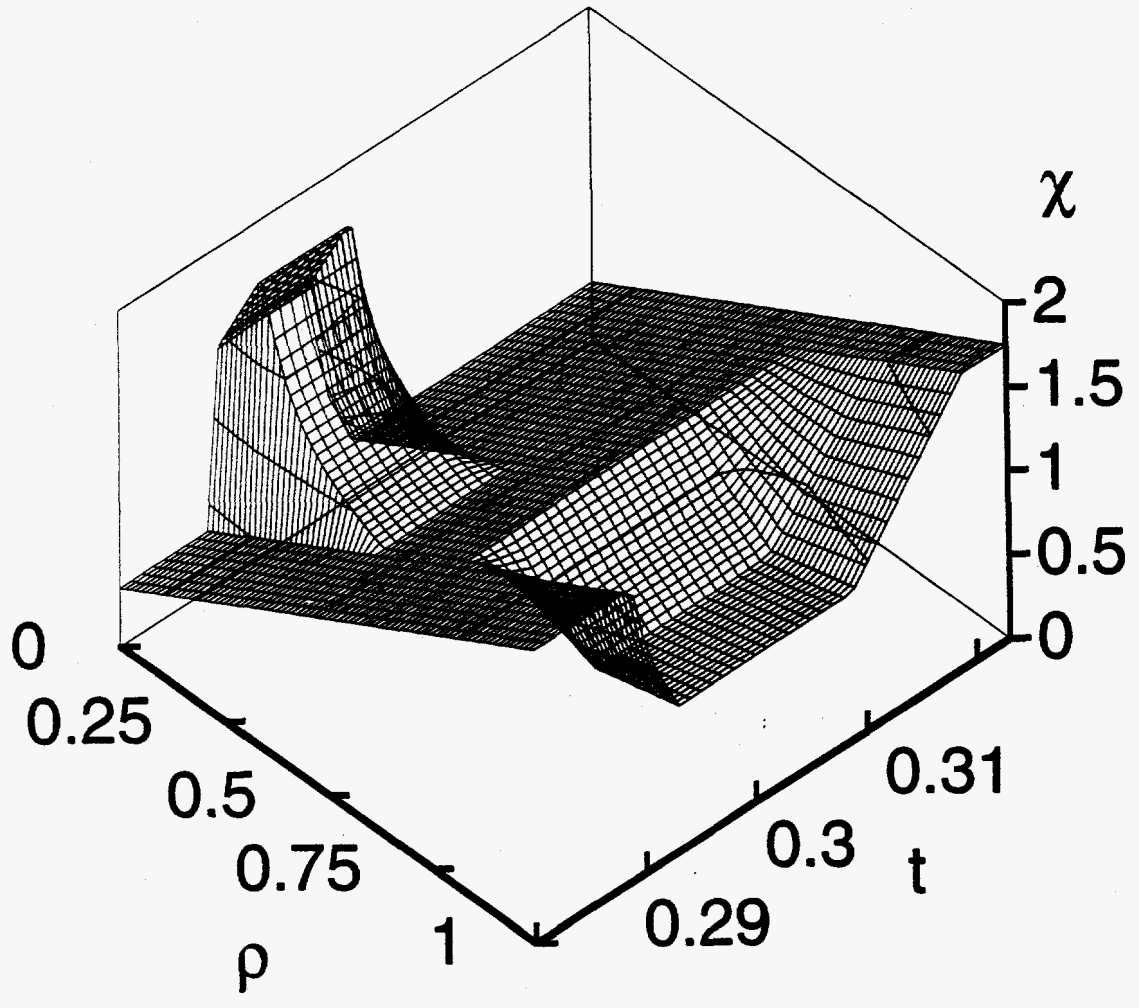

Fig. 3 $\chi_e(\rho,t)$ for the transport model shown in Fig. 2 as light lines -- core degradation and edge improvement.

The effect certainly depends on the amplitude of the voltage applied. The temperature decrease becomes smaller at lower voltages. It disappears at voltages (current ramp rates) half

that shown in Fig. 1. Furthermore, if the initial current is raised to 200 kA, which produces clear sawteeth, no decrease in central temperature is found.

The plasma response to a fast current increase is the complete inverse of that found for the cold pulse from impurity ablation, for which the core χ_e improved and the edge value increased greatly. The behavior in both cases is clearly nonlocal in that the core χ_e changes on a submillisecond time scale in the absence of any change in local fluid variables. The combination of "cold pulse" and current step experiments strengthens the interpretation of the response as a nonlocal transport effect as opposed to an idiosyncratic effect in a single experiment. The nonlocal effects require some sort of global coupling and communication in the transport process. Furthermore, the combination of transport improvement with degradation and the complementarity between edge cooling and heating results suggest some sort of constraint or conservation principle. A condition related to the current or current profile is certainly one possibility. However, the time scales for the duration of the transient nonlocal changes in transport coefficients are typically of order 10 msec or less in these experiments, much less than current profile relaxation times. (The exception is the longer duration of edge improvement in Fig. 3, but that may be an artifact reflecting the general change in equilibrium $\chi_e(\rho)$ for the higher-current, lower-q final state. The modeling has concentrated on the first 20 msec of the current ramp. A careful analysis of the slow approach to the new equilibrium has not yet been completed.)

Resolution of these questions will require many additional experiments. Among the most obvious are searching for the associated changes in turbulence with the Heavy Ion Beam Probe. An edge heating process independent of current would also be valuable to separate some aspects of current versus temperature. TEXT has sufficient ECRH heating power to match the ohmic increment of these experiments, but an X-mode launch system would be necessary to obtain adequate absorption for the edge plasma conditions. Faster current ramp rates -- higher voltages -- are also needed to determine whether the effect truly disappears at lower q or merely requires a stronger drive at lower q.

Work supported by the U.S. Department of Energy under Grant No. DE-FG05-88ER-53267.

[1] K.W. Gentle *et al.*, Phys. Rev. Lett. **74**, 3620 (1995).

[2] K.W. Gentle *et al.*, Phys. Plasmas **2**, 2292 (1995).

[3] J.G. Cordey *et al.*, Plasma Phys. and Contr. Fusion **36**, A267 (1994).

BES DENSITY FLUCTUATION MEASUREMENTS ON TEXT-U AND COMPARISON WITH OTHER DIAGNOSTICS.

Yuri Y. Karzhavin, R. D. Durst,[1] Roger D. Bengtson, R.V. Bravenec, D. L. Brower,[2] G. Cima, R.J. Fonck,[1] J.W. Heard, J.S. Kim,[1] A.N. Nikitin, A. Ouroua, E.J. Powers, D.R. Roberts, C. Watts,[3] A.J. Wootton.

Fusion Research Center, The University of Texas at Austin , U.S.A.;

[1] University of Wisconsin, Madison, U.S.A.; [2] University of California, Los Angeles, U.S.A.; [3] Auburn University, Auburn, AL, U.S.A.

1. Introduction

There have been many efforts in the past decade to measure plasma turbulence to assess the importance of fluctuations to the observed anomalous transport in tokamaks. Experiments on TEXT [1] confirmed that electrostatic fluctuations indeed can explain the observed anomalous flux in the plasma edge. A similar statement cannot be made about the plasma core [2] due to inconsistencies between far-infrared (FIR) scattering [3] and heavy-ion beam probe (HIBP) [4] measurements of the poloidal wave-number spectra. In an attempt to resolve this issue a recently developed beam-emission spectroscopy (BES) [5] diagnostic for local plasma density fluctuation measurements was installed on TEXT-Upgrade (TEXT-U).

The BES diagnostic is based on measurements of fluctuations in the intensity of the fluorescent emission from a neutral beam injected into the plasma. The TEXT BES system uses a diagnostic neutral beam (DNB) of helium to separate the beam emission from edge H_α (D_α) light [6]. Application of cryogenically cooled (to -50° C) avalanche detectors results in considerably lower dark noise of the detector circuits and a signal-to-noise ratio of the detectors is almost at the photon noise limit. Each of eight BES channels collects light from a roughly rectangular plasma volume of dimensions 7 mm (poloidal) × 15 mm (radial) × 50 mm (toroidal). The poloidal and radial separations of the volumes are 10 mm and 17 mm, respectively. This implies an ability to resolve wave numbers $k_\theta \lesssim 5$ cm^{-1} and $k_r \lesssim 2$ cm^{-1}.

Density fluctuation measurements in TEXT-U plasmas have been performed by the BES system in limiter hydrogen (deuterium) plasmas with $1.5\ T \le B_T \le 2.3\ T$, $1 \times 10^{13} \le \bar{n}_e \le 4 \times 10^{19}$ m^{-3}, $150\ kA \le I_p \le 250\ kA$ over the plasma region $0.5 \lesssim r/a \lesssim 1.1$. The data were compared with results from Langmuir probes at the plasma periphery and with FIR scattering and the HIBP in the interior.

2. Experimental results

Figure 1(a) shows the cross-power and cross-phase spectra between two channels located at $r/a \cong 1.05$ (in the SOL) and poloidally separated by 1 cm. The limiter was located at r = 27 cm. The spectra exhibit broadband ($\Delta f/f \sim 1$) fluctuations propagating in the ion diamagnetic drift (IDD) direction. Characteristics of the turbulence are poloidal power-weighted wave number $\langle k_\theta \rangle \approx -1.5 \div 2$ cm^{-1} and poloidal phase velocity (lab frame) $\langle V_{ph} \rangle \approx -0.8 \div 1.33$

km/s. Measured parameters of the turbulence are consistent with Langmuir probe observations in the same shots.

Moving the BES channels inwards (r/a ≅ 0.9), the cross-power spectrum acquires a shape with two characteristic features [Fig. 1(b)]. One, a feature at low frequencies ($f \lesssim 50$ kHz) propagates in the IDD direction (as in the SOL), and a broadband feature with $f \gtrsim 50$ kHz which propagates poloidally in the electron diamagnetic drift (EDD) direction. Parameters of the ion mode are $\langle k_\theta \rangle \cong -0.8 \div 1$ cm^{-1} and $\langle V_{ph} \rangle \cong -2$ km/s (lab. frame). The broadband electron mode is characterized by $\langle k_\theta \rangle \cong 2$ cm^{-1} and $\langle V_{ph} \rangle \cong 3.0$ km/s at the typical average frequency of 100 kHz . Note that at frequencies close to 60 kHz the powers of these two modes are about equal and the cross-phase is changing from the IDD to the EDD direction.

Data at r/a ~ 0.5 is presented in Fig. 2. The shape of the cross-power spectrum is in general the same as at the edge although the fluctuation power is almost ten times lower. In contrast to the data at r/a ≈ 0.9 (Fig. 1(b)) there is an apparent lack of clear propagation in the IDD direction of the feature at low frequencies ($f \lesssim 25$ kHz) and the appearance of two features at ~75 and ~125 kHz. The phase shifts measured for all three features are very small. The remainder of the spectrum propagates in the EDD direction at a phase velocity of ~ 3 km/s (accounting for finite emission-volume effects [8]), consistent with electron drift waves and FIR scattering results [3], and exhibits a poloidal correlation length of $l_\theta \approx 0.8$ cm. The fluctuations at low frequencies ($f \lesssim 25$ kHz) at this radial location apparently are dominated by noise on the DNB and perhaps sawteeth, during this experimental series. It is consistent with the observed zero phase and long poloidal correlation lengths $l_\theta \approx 4.5$ cm. This noise may dominate any ion feature that might exist. At the periphery ($r/a \gtrsim 0.7$), the stronger fluctuations dominate the DNB noise.

Although they also exhibit near-zero phases, the features at ~75 and ~125 kHz do not appear to be due to DNB noise by virtue of the relatively small values of measured $l_\theta \approx 1.5$ cm. A radial scan shows that these low-k features are localized in the confinement zone. Bi-coherence analysis has shown that these feature are not different harmonics of the same mode. Future experiments will address the dependences of these features on the plasma parameters.

Comparisons were made of the ion features for shots with chord-averaged densities of 1.5 to 3.5×10^{19} m^{-3}, keeping other plasma parameters the same ($I_p = 200$ kA, $B_T = 2$ T). Power of the fluctuations for a single BES channel located at r/a = 0.85 is shown in Fig. 3. The observed increase of the fluctuation power of the ion feature with density gives rise to the hypothesis that this ion feature is related to an η_i mode, as speculated earlier from FIR scattering results on TEXT [3]. In addition, the amplitude of the mode decreases upon onset of the improved confinement regime on TEXT-U reported earlier [7].

A special experiment was devoted to comparison of fluctuation data measured by different fluctuation diagnostics. Although a direct comparison is hampered by the fact that different diagnostics observe different locations in the plasma, initial results may be presented

assuming poloidal symmetry of $\langle k_\theta \rangle$ and $\langle V_{ph} \rangle$. Figures 4(a) and 4(b) show radial profiles of $\langle k_\theta \rangle$ and $\langle V_{ph} \rangle$, respectively, measured by BES, the HIBP, and Langmuir probes for $0.5 \leq r/a \leq 1.1$ in the same experimental run. Results of FIR scattering are taken from Ref. [3]. HIBP data for this experiment are shown as the shaded region in Fig. 4, while the filled circles refer to results from TEXT [2,4]. The value of the phase velocity at r/a = 0.6 in Ref. [2] was 13.3 km/s. Interpretation of the HIBP measurements is complicated by the oblique orientation of the sample volume with respect to the poloidal direction. The lower boundary for $<V_{ph}>$ and the upper boundary for $<k_\theta>$ are obtained assuming no propagation in the radial direction and taking the shortest poloidal distance between sample volumes as the sample-volume separation.

In the SOL, BES measurements are consistent with Langmuir probes. In the interior, all of the diagnostics observe a broad spectrum centered around 100 - 150 kHz, with fluctuations propagating in the EDD direction. Measured poloidal wave numbers and phase velocities are in good agreement. The data is consistent with a drift-wave model. HIBP phase velocities are consistent with those measured by FIR scattering and BES assuming $\langle k_r \rangle \sim 0$. Low $\langle k_r \rangle$ was confirmed by BES (although the emission-volume orientation was not optimal). The ion feature seen by BES near the edge is similar to an ion feature reported by FIR scattering and has similar dependances on the plasma parameters. The clear propagation of the low-frequency mode in the IDD direction is not evident in HIBP data and this difference is a subject of future studies.

3. Conclusions

An eight-channel BES system has been installed on TEXT-U capable of measuring poloidal and radial density fluctuations with $k_\theta \lesssim 5$ cm^{-1} and $k_r \lesssim 2$ cm^{-1} in the plasma region $0.5 \lesssim r/a \lesssim 1.1$. Measurements of the interior fluctuations in the standard TEXT-U regime 2 T / 200 kA / 2×10^{19} m^{-3} / H (D) show that at higher frequencies ($f \gtrsim 50$ kHz) data are consistent with drift-wave-like turbulence [2]. At low frequencies fluctuations propagate in the ion diamagnetic drift direction and have similar characteristics and plasma-parameter scalings as measured by FIR scattering [3]. In addition, two fast low-k_θ electron modes are detected at ~75 kHz and ~125 kHz in the plasma confinement region. Future experiments will address the natures of the fast electron features and the ion mode.

4. References

1. A.J. Wootton et al., Phys. Fluids B **2** (12) 2879 (1990).
2. R.V. Bravenec et al., Phys. Fluids B **4** (7) 2127 (1992); Nucl. Fusion **31** (4) 687 (1991).
3. D.L. Brower, W.A. Peebles, N.C. Luchmann, Jr., Nucl. Fusion **27** (12) 2055 (1987).
4. T.P. Crowley et al., Nucl. Fusion **32** (8) 1295 (1992).
5. R.J. Fonck, P.A. Duperrex, S.F. Paul, Rev. Sci. Instrum. **61** (11) 3487 (1990).
6. R.D. Durst et al., Rev. Sci. Instrum. **66** (1) 842 (1990).
7. A.J. Wootton et al., 15th IAEA Conf., IAEA-CN-60/A2/4-P-9, Seville, Spain (1994).
8. D.W. Ross et al., Nucl. Fusion **31** (7) 1355 (1991).

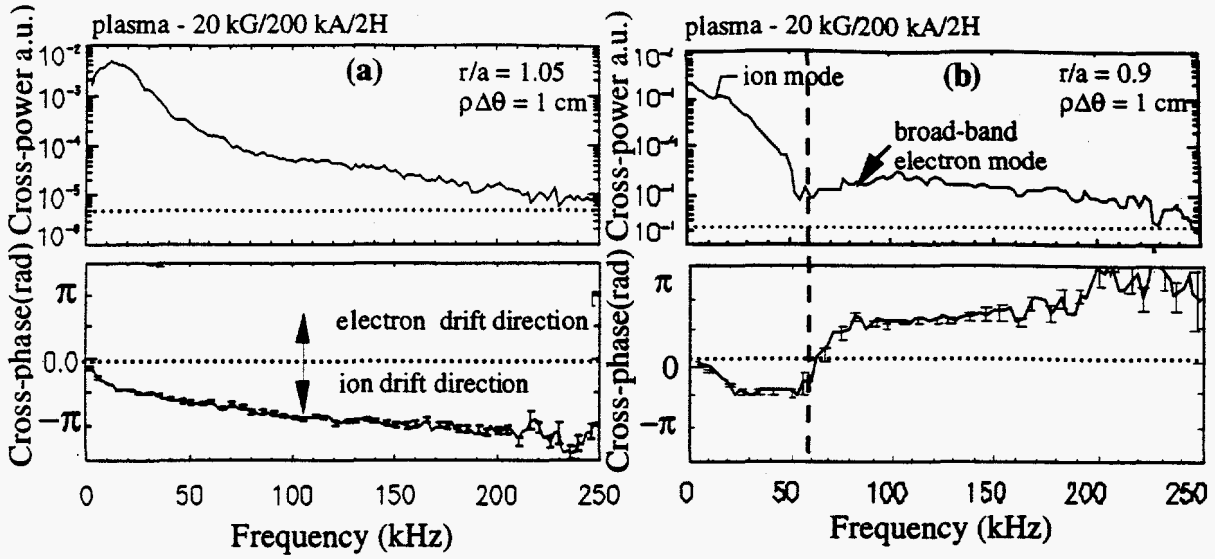

Fig. 1. Cross-power and cross-phase frequency spectra between two BES channels poloidally separated by 1 cm. a) r /a = 1.05 b) r /a = 0.9. Plasma conditions: 20 kG/200kA/2H.

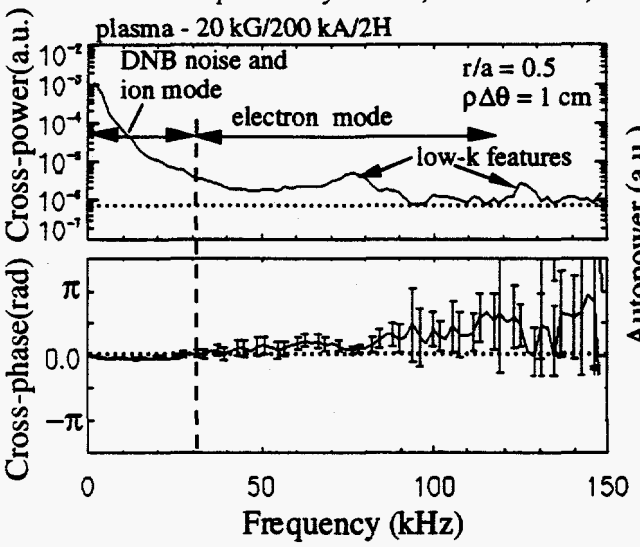

Fig. 2. Cross-power and cross-phase spectra at r/a = 0.5.

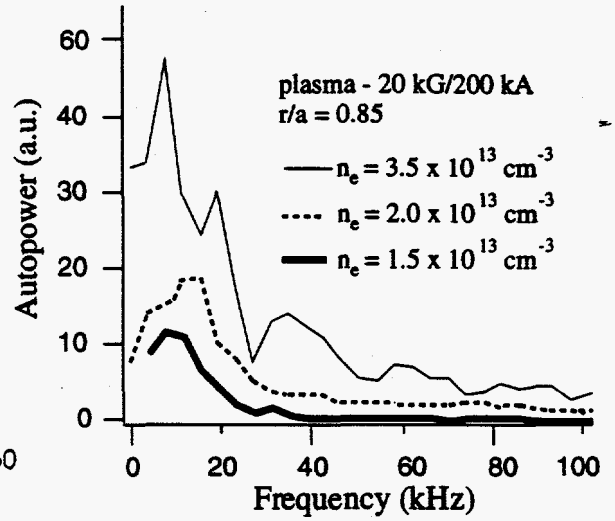

Fig. 3. Comparison of fluctuation power of the ion feature in regimes with different densities.

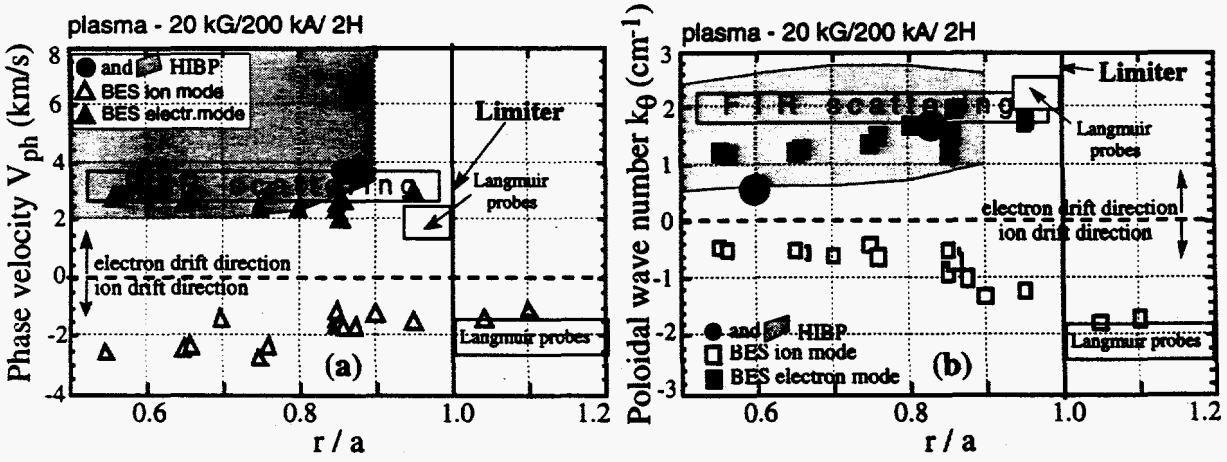

Fig. 4. Radial distributions of a) poloidal phase velocity, b) poloidal wave number of the density fluctuations measured by BES, FIR, HIBP, and Langmuir probes in TEXT-U.

The SOL in Diverted Discharges in the Texas Experimental Tokamak (TEXT)

William L. Rowan, Roger. D. Bengtson, Xavier Bonnin, R. V. Bravenec,
T. P. Crowley,† K. W. Gentle, J. W. Heard,† P. D. Hurwitz, A. Ouroua,† P. E. Phillips,
B. Richards, K. A. Schroder, P. M. Schoch,† D. J. Storek, and D. L. Winslow
Fusion Research Center, The University of Texas at Austin, Austin, Texas 78712, USA
†Rensselaer Polytechnic Institute, Troy, NY 12180, USA

1. Introduction

In the Texas Experimental Tokamak, TEXT-U, tokamak plasmas are produced in diverted or limited configurations [1] in a boronized or unboronized vacuum vessel and can be heated with 600 kW of ECRH. SOL experiments are yielding interesting results on the source of plasma turbulence, on recycling and impurity asymmetries near the divertor tiles, and on asymmetries in density fluctuations. Because electrostatic turbulence appears to be the mechanism for cross-field transport in the SOL, the main goal is to identify possible turbulence drives. SOL simulations will eventually be used to compare predicted drives to experiment. Until then, the simulations are being used to investigate up-down asymmetries near the divertor tiles.

2. Experiments to Identify the Turbulence Drives

Cross field transport in the SOL is well correlated with the transport due to electrostatic turbulence. The source of the turbulence remains elusive, but the turbulence properties have been identified. One of these may be particularly valuable. The magnitude of $k_{||}$ relative to k_θ may suggest a spatial location for the drives. Since parallel wave numbers for the turbulence are small, the turbulence drives may be well separated from the point of observation -- as far away as the divertor plates or the limiter. Hence, turbulence may be due to atomic drives resulting from ionization [2] or radiation [3] near the divertor plates or limiter or due to curvature drives [4] that depend on unfavorable magnetic curvature along only one limited region of a magnetic field line.

2.1 Ionization Drive

To understand the ionization drive, simply consider the electron source, $n_e S n_0$, due to the ionization of neutrals. Clearly, a density fluctuation will act through this term to increase the level of fluctuations. The drive was examined in detail [2] to produce both a critical level of ionization for the instability to exist and a prediction of the associated particle transport.

To search for this drive, the TEXT-U experiments were conducted in a poloidally limited discharge to make the drive as large as possible. In this discharge, the local ionization produced near the toroidally localized limiter is as high as can be produced in TEXT-U. In a series of discharges, the electron density was increased shot by shot. As the density increased, the ionization increased, but the relative fluctuation level was independent of the increase. Though one conclusion is that the ionization drive does not exist, a second is that the fluctuation level is simply saturated. In a second experiment, the fluctuation level was measured in close proximity to the toroidally localized limiter and as a function of distance from it. Because the neutral density is a decaying function of distance from the limiter, this was a measurement of fluctuation level as a function of neutral density along a magnetic field line. The fluctuation level was independent of the local ionization rate. Though interesting, this result may simply reflect the magnitude of $k_{||}$. Finally, the transport due to the ionization drive was estimated. The predicted transport is directed inward and more than an order of magnitude smaller than the measured transport which is directed outward. It is concluded that the ionization drive does not play a role in TEXT-U and may not exist at all. The latter point is consistent with a recent critique [5] of the original theory.

2.2 Radiation Drive

If the radiated power, P_{rad}, is represented in terms of the electron density, n_e, the impurity density, n_z, and the cooling rate, I_z, in the usual way as

$$P_{rad} = n_e \sum_z (n_z I_z) ,$$

then the growth rate for this instability is [3]

$$\gamma = \frac{2\, n_z}{3} \left(\frac{2\, I_z}{T_e} - \frac{\partial I_z}{\partial T_e} \right).$$

In TEXT-U experiments, the effects of the second term were sought. Were the cooling rate to decrease with increasing T_e (as suggested in the original work on this drive [2] following results from calculation based on coronal models, [6] for example), then the instability would grow. In TEXT-U experiments, T_e in the plasma periphery was modulated with ECRH. The plasma radiation appeared to be in phase with the temperature at the plasma edge, hence the second term of the above equation is not destabilizing. Furthermore, this might almost have been expected because the inference of a destabilizing influence of that second term is based on a coronal model for impurities which, of course, omits transport.

2.3 Curvature Drive

The toroidal curvature of the magnetic field lines may be a source for turbulence in tokamaks [4]. On the open field lines in the SOL, some fluid modes may be unstable for the appropriate average curvature of the magnetic field lines with respect to the pressure gradient. In a tokamak, curvature is stabilizing on the inner side of the torus (on the high field side of the poloidal cross section) and destabilizing on the outer side (on the low field side).

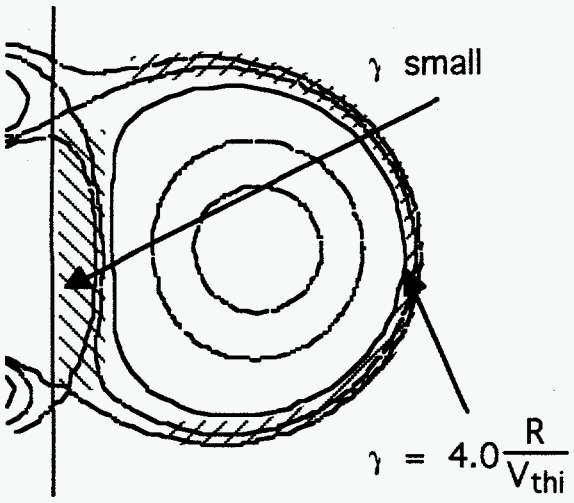

Figure 1. Curvature drive in a DN discharge

On TEXT-U, curvature drives can be studied by comparing turbulence measurements in two different configurations, poloidally limited and double null (DN). In the double null configuration (see figure 1), the SOL on the high field side (favorable curvature) is effectively isolated from that on the low field side (unfavorable curvature). The growth rate, γ, for the curvature instability at $k_{||}=0$ in each of the two configurations can be estimated using a simple model [4] due to Garbet. The results are shown in Figure 1 where R is major radius, and V_{thi} is ion thermal velocity. For the poloidally limited configuration, $\gamma = 2.5 \frac{R}{V_{thi}}$ for the entire SOL. As shown in figure 2, the turbulence level is as predicted, higher on the low field side (LFS) than on the high field side (HFS). This is consistent with previous findings [7]. A similar experiment in a limited configuration in TEXT-U gave essentially the same fluctuations on both the HFS and on the LFS.

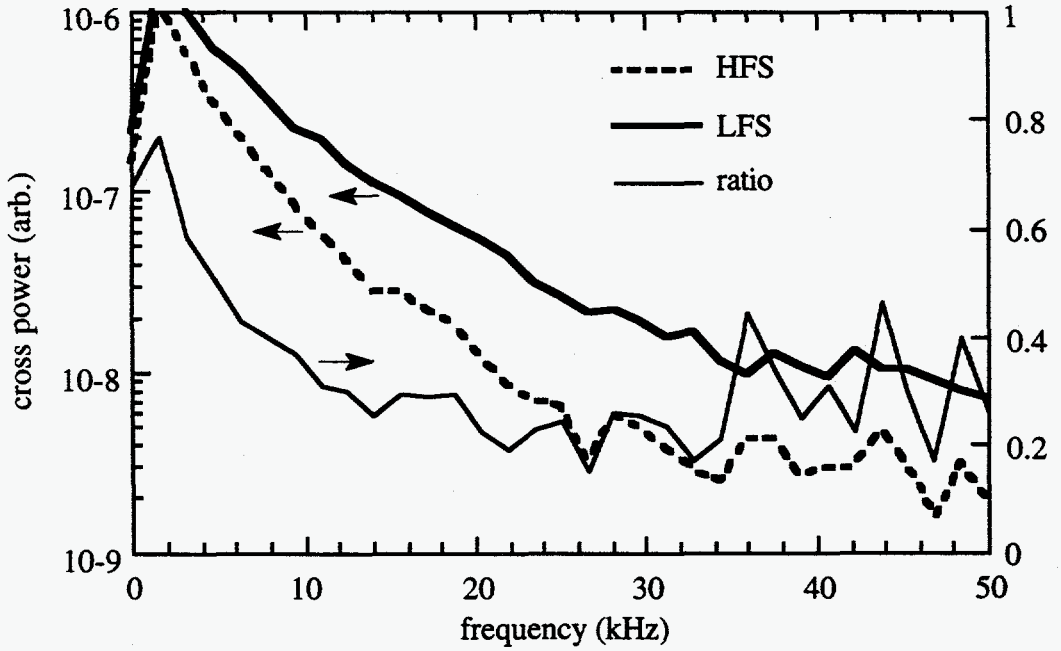

Figure 2. Comparison of HFS and LFS turbulence in a diverted discharge

3. SOL simulation. A study of up-down asymmetry.

In equatorial single-null discharges (see figure 3a), there is an up-down asymmetry in D_α and impurity emission from the vicinity of the divertor plate. The spectroscopic viewing chords are shown in figure 3a. The radiance measurements and simulations are in figure 3b. The tangent radius of 3b is measured with respect to the center of the magnetic configuration.

The degree of asymmetry is independent of plasma current direction, but decreases and eventually reverses with increasing n_e. The divertor plate construction and the magnetic configuration are up-down symmetric, so this configuration is ideal for study of the plasma drives for up-down asymmetries. In a first attempt to understand the measured asymmetry, the B2-Eirene [8] plasma simulation code was used to examine the impact of the $\nabla T \times B$ drift on D_α emission at the divertor plate. The inclusion of the drift correctly predicts the sign of the asymmetry. Addition of carbon impurities (drift + C of Fig. 3b) further enhances the asymmetry and improves agreement with the experimental data. The increased effect of the $\nabla T \times B$ drift with carbon may simply be due to enhancement of the temperature gradient via radiative losses. However, the dependence on density is not yet understood.

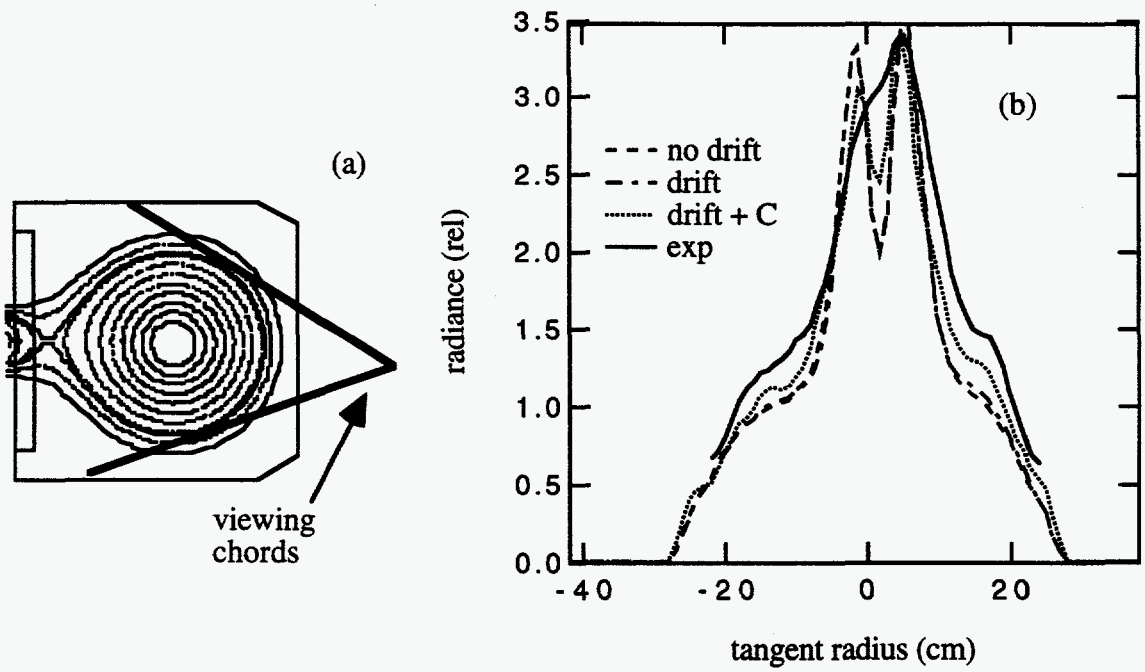

Figure 3. D_α emission: simulation and experiment.

Acknowledgements

This work was supported by the U. S. Department of Energy under grant DE-FG05-88ER-53267 to The University of Texas.

References

[1] W. L. Rowan, et al., J. Nucl. Mater. 220-222, 668 (1995)

[2] A. S. Ware, et al., Phys. Fluids B 4, 877 (1992)

[3] D. R. Thayer and P. H. Diamond, Phys. Rev. Lett. 65, 2784 (1990)

[4] X. Garbet, et al., Nuclear Fusion 31, 967 (1991)

[5] D. W. Ross, Phys. Plasmas 1, 2630 (1994)

[6] D. E. Post, et al., Atom. Data Tables 20, 397 (1977)

[7] M. Endler, et al. J. Nucl. Mater. 220-222, (1995).

[8] R. Schneider et al., J. Nucl. Mater. 196-198, 810 (1992)

Confinement and Related Studies in TEXT

A. J. Wootton, R. Bengtson, R. Bravenec, D. Brower[1], G. Cima, K. Connor[2], T. Crowley[2], P. Edmonds, R. Durst[3], R. Fonck[3], A. Fujisawa[4], R. Gandy[5], H. Gasquet, Gentle, G. Geruzzi[6], G. Hallock, J. Heard[2], P. Hurwitz, J. Jagger, Y. Jiang[1], Y. Karzhavin, S. McCool, W. Miner, A. Ouroua[2], D. Pavlosky, E. Powers, P. Phillips, B. Richards, D. Roberts, D. Ross, W. Rowan, P. Schoch[2], D. Sing, E. Solano, R. Steimle, D. Terry, J. Uglum, C. Watts[5], D. Winslow, B. Zhang, S-B. Zheng.

University of Texas at Austin, Austin, TX 78712, USA

1: The University of California, Los Angeles, CA 90024-1597, USA. 2: Rensselaer Polytechnic Institute, Troy, NY 12181, USA. 3: The University of Wisconsin at Madison, Madison, WI 53706, USA. 4: National Institute for Fusion Science, Nagoya, Japan. 5: Auburn University, Auburn, AL 36849, USA. 6: Association Euratom-CEA sur la Fusion, Departement de recherches sur la fusion controlee, Centre d'etudes nucleaires de Cadarache, Saint-Paul-le Durance, France.

Operational regimes

The tokamak TEXT (major radius $R \approx 1.05$ m, minor radius $a \leq 0.3$ m) operates with either circular or separatrix-limited discharges, with 600 kW of outside-launch electron-cyclotron heating (ECH) at ≈ 60 GHz. Trimethyl boron and He glow discharges, used for vessel wall preparation, produce ohmic loop voltages $\approx$ 1V/turn and $\approx 50\%$ improvement in the ohmic energy confinement time.

MARFES are produced either spontaneously near the density limit, or controlled by C ablation followed by neon puffing. A high radiation region exists in the high field upper quadrant. In the high field lower quadrant, between r = 15 and 20 cm (the poloidal extent is as yet unknown) there is a region with high normalized density fluctuation level $\tilde{n}/n \approx 5\%$. Normal discharges have $\tilde{n}/n < 2\%$ here. This region is well separated from the usual scrape-off layer (SOL) turbulence at r > 27 cm, and should allow a distinction to be made between different turbulence drives. On a subset of the spontaneous MARFE discharges the high edge density collapses, producing improved particle confinement time τ_p. and reduced $\tilde{n}/n$.

H-mode-like transitions in limited plasmas are observed with edge safety factor $q_a \approx 3$ and plasma current $I_p \approx 250$ kA (ohmic power $P_{oh} \approx 300$ kW) when also applying over 300 kW of central ECH. These are dithering transitions induced by sawtooth crashes, which display a D_α drop, a τ_p increase, and ELM's. Transitions are only observed when limited on the toroidally localized top or bottom limiters; no transitions are found with discharges limited by the high-field inner wall (a toroidal belt) or in diverted configurations.

The improvement in energy confinement time following the transition is that expected from the density dependence of the L mode, which is approximately consistent with the

Goldston quadrature fit. No edge transport barrier (steep gradient) is found. A preliminary analysis shows that when ECH is first applied (L mode) the particle diffusivity D increases and the inward pinch velocity v decreases. The increase in τ_p in the H mode is a consequence of a reduced D. There is preliminary evidence for a poloidally asymmetric plasma potential change, and $\tilde{n}/n$ increases.

Interior turbulence and transport

Measurements of interior electrostatic turbulence show a distinct poloidally asymmetric feature [1]. Figure 1 shows power spectra of $\tilde{n}/n$ for an ohmic discharge obtained with the heavy ion beam probe (HIBP) from four sample-volume locations. A feature is apparent on the low-field (large major-radius) side in density $\tilde{n}$ (HIBP) and temperature $\tilde{T}_e$ (electron cyclotron emmission ECE) fluctuations. It propagates in the electron diamagnetic drift direction, has a frequency spread $\Delta f / f \approx 60kHz/150kHz$, and a wave vector $k_\theta \approx 1.5$ cm^{-1}. The associated fluctuating power decreases with increasing density. With centrally localized ECH the central temperature T_e increases, the temperature scale length $L_T = T_e(\partial T_e / dr)^{-1}$ decreases and the density scale length increases $L_n = n(\partial n / dr)^{-1}$ (the density profile can become hollow). At the same time the fluctuating power in the feature near the axis decreases. Increasing $\tilde{n}/n$ is well correlated with an increasing theoretical growth rate of the dissipative trapped electron mode (DTEM) [2]. The same feature, observed using ECE as $\tilde{T}_e / T_e \leq 1.5\%$, is correlated with the small gradient changes associated with the outward propagation of a sawtooth crash. Insufficient data exist to calculate the crash-induced changes in the theoretical DTEM growth rate. However assuming $\tilde{T}_e / T_e \propto (L_T / a)^\alpha$ then $\alpha < 0$ is different for the equilibrium than during the crash transit.

Previously we showed that the measured electrostatic turbulence with $\bar{k}_\theta \approx 1.5$ cm^{-1} was insufficient to explain the total electron heat flux deduced from a profile power balance analysis [3]. However it was estimated that turbulence with $\bar{k}_\theta \approx 3$ cm^{-1} could be consistent with the data and explain electron energy transport if the effects of finite sample volumes (filtering k < 2 cm^{-1}) were accounted for. This problem is exacerbated by the new data which shows that at the top and bottom of the plasma there is no significant power with $\bar{k}_\theta < 5$ cm^{-1}.

Concerning the importance of magnetic turbulence, we used ECH together with the inductive toroidal electric field to produce non-thermal electrons with a parallel energy ≈ 0.1 MeV [4]. The spatial distribution of these fast electrons, monitored using a vertical viewing ECE system, is dependent on a spatial diffusivity D_{fast}, itself assumed dependent on a magnetic fluctuation level. This magnetic fluctuation level is insufficient to explain electron energy transport; assuming $\chi_e / D_{fast} = v_{the} / v_{\|fast}$. with v_{the} the electron thermal velocity and $v_{\|fast}$ the fast-electron parallel velocity, the thermal electron diffusivity $\chi_e \approx 0.3 m^2 s^{-1}$.

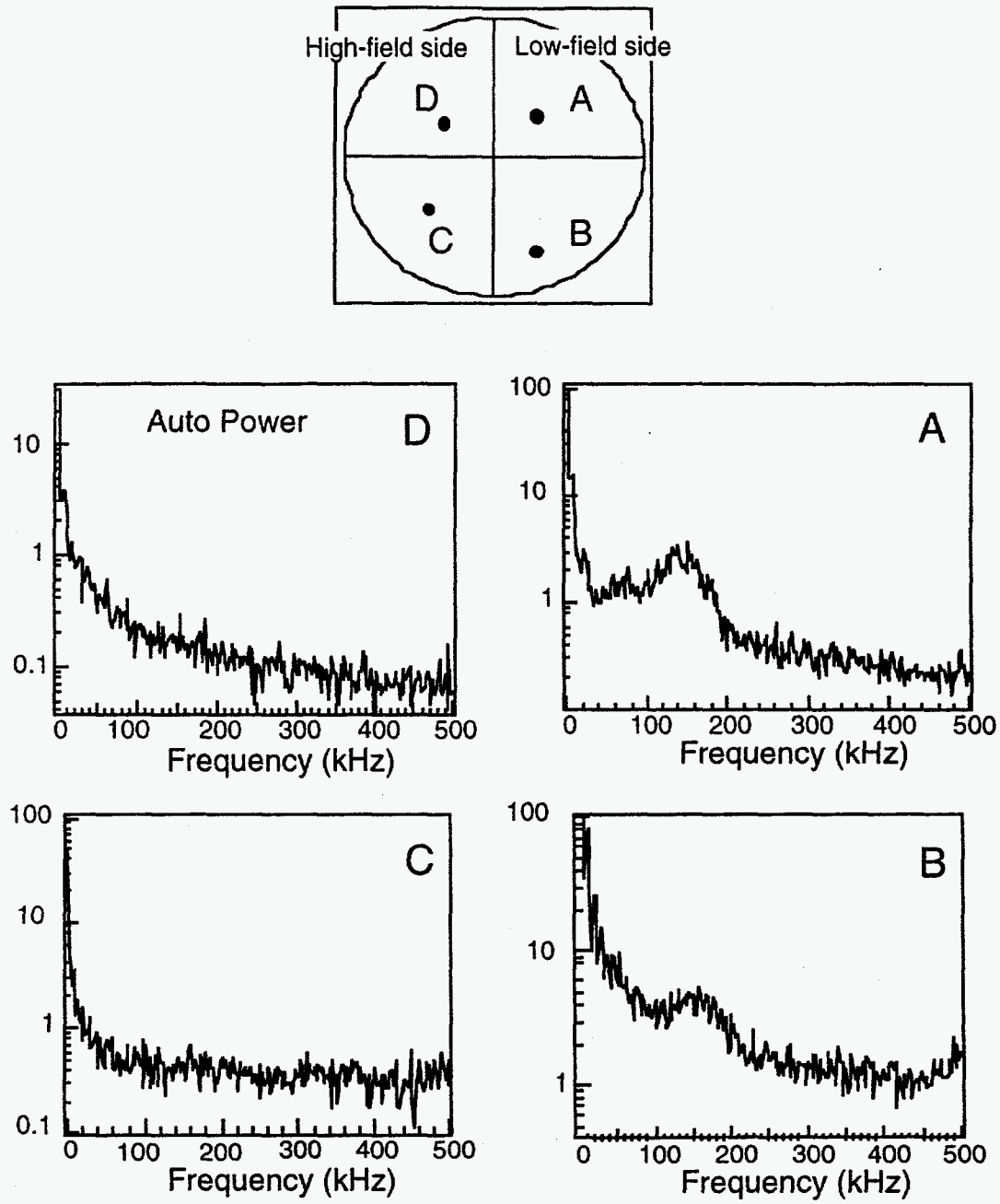

Figure 1. Power spectra of normalized density fluctuations at different poloidal locations, showing a poloidally asymmetric structure (at ≈ 150 kHz) on the low-field side of a reference TEXT-U limiter discharge.

There is no evidence in normal discharges that temperature flat spots (i.e. regions of large χ_e, produced e.g. by magnetic islands) are responsible for the time averaged χ_e. The data shown in Figure 2 as L_{Te}^{-1} against plasma minor radius were obtained by moving the plasma horizontally while viewing with ECE detectors. The solid line represents a fit to single detector data. The broken line shows data from two detectors, where the signal difference directly provides the gradient. Outside the q = 1 surface, at r ≈ ± 5 cm, there is no evidence for flat spots with width > 0.5 cm (the spatial resolution of the technique).

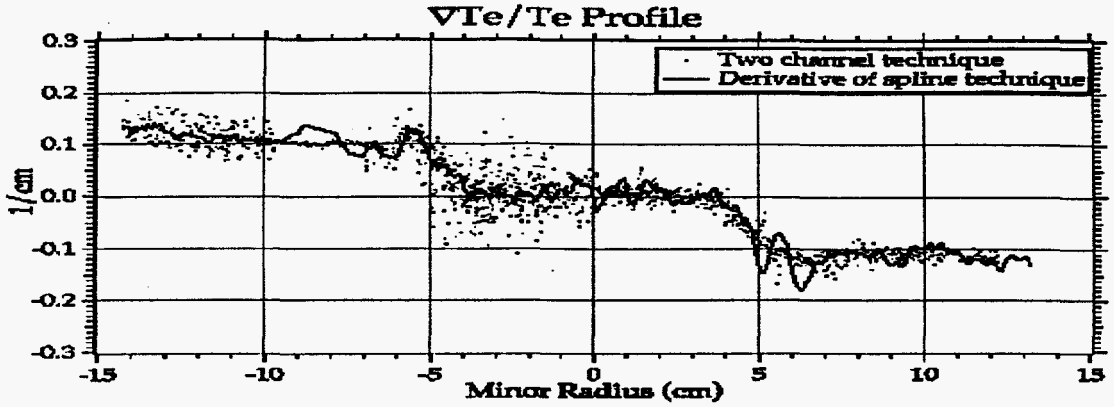

Figure 2. The inverse gradient scale length from a two point and single point ECE measurement.

Edge turbulence and transport

Measurements of fluctuations in the SOL are directed at investigating drive mechanisms [5]. Concerning radiation drives, correlations between radiation fluctuations and both temperature and density fluctuations have been sought but not found above noise levels. During modulated ECH the equilibrium changes to P_{rad} and T_e are in phase, implying no thermal instability. Experiments in which H_α or D_α fluctuations are measured as the particle source and density are varied show no evidence of an ionization drive. Initial experiments utilizing and comparing the effects associated with steel and boron nitride boundaries show that edge turbulence may be sensitive both to the boundary material, presumably the material conductivity, and the direction of the field line, presumably the magnetic curvature. That curvature may be important is also deduced from experiments in a double-null, separatrix-defined, D-shaped discharge. Here the edge turbulence is found to be smaller on the high-field side (where the field lines experience only good curvature) than on the low-field side. This asymmetry is not found for circular, limited discharges.

Conclusions

TEXT now produces different operational regimes, including limiter H mode. These regimes will be used to study links between turbulence, transport and E_r. In the interior a poloidally asymmetric turbulence feature, with some characteristics similar to those of the DTEM, has been isolated. In the edge magnetic curvature appears important as a turbulence drive.

References

[1] A. Fujisawa et al., Fusion Research Center Report FRCR #466, (1995).

[2] W. Horton, Phys. Fluids **19** 711 (1976).

[3] G. Cima et al., Phys. Plasmas **2** 720 (1995).

[4] R. F. Steimle et al., Fusion Research Center Report FRCR #469, (1995).

[5] P. Hurwitz, "Optical Imaging of Turbulent Fluctuations in TEXT-U", Ph.D. Thesis, University of Texas at Austin, 1995.